The Warming Physics of Tropic World: Part 1 Mean State

Dennis L. Hartmann[1], Brittany D. Dygert[1], Qiang Fu[1] and Peter N. Blossey[1]

[1]Department of Atmospheric Sciences, University of Washington, Seattle, Washington 98195

Key Points:

- The SST contrast increases with warming, primarily because the clear-sky greenhouse effect feedback is stronger in the warm region.
- As the climate warms, the integrated cooling rate of the atmosphere increases by moving upward into lower pressures and increasing in strength, giving a more top-heavy cooling profile.
- The more top-heavy cooling rate profile results in increased cloud ice as the climate warms.

Corresponding author: Dennis L. Hartmann, `dhartm@uw.edu`

Abstract

Warming experiments with a uniformly insolated, non-rotating climate model with a slab ocean are conducted by increasing the solar irradiance. As the climate warms, the surface temperature contrast between the warm, rising and cooler, subsiding regions increases, mostly as a result of the stronger greenhouse effect in the warm region. The convective heating rate becomes more top-heavy in warmed climates, producing more cloud ice, principally because the radiative cooling rate moves to lower pressures and increases. To produce this more top-heavy convective heating, precipitation shifts from the convective to the stratiform parameterization. The net cloud radiative effect becomes more negative in the warm region as the climate warms. At temperatures above about 310K surface temperature contrast begins to decline, and the climate becomes more sensitive. The reduction in SST contrast above 310K again appears to be initiated by clear-sky radiative processes, although cloud processes in both the rising and subsiding regions contribute. The response of clear-sky outgoing longwave to surface warming begins to accelerate in the region of rising motion and decline in the region of subsidence, driving the SST contrast to smaller values. One-dimensional simulations are used to isolate the most relevant physics.

Plain Language Summary

A global model of a non-rotating Earth with an ocean that stores heat but does not transport it is run to equilibrium with different values of globally uniform solar heating. Despite the complete uniformity of the system, it still develops regions of warm sea surface temperature where rain and rising motion occur, and regions with downward, subsiding air motion where rainfall does not occur. These contrasts look very similar to what is observed in the present-day tropics. As the climate is warmed from current temperatures toward warmer temperatures, the warm regions warm faster, mostly because the rising regions contain more water vapor. The clouds rise to higher altitudes in the warmer climates, and produce more cloud ice. These changes are shown to arise from well-understood physical processes that are expected to operate in nature.

1 Introduction

The tropical atmosphere exhibits regions of consistently active deep convection, where the SST is generally higher and the free troposphere is more humid, and regions where deep convection is rare, the air is dry, and the SST is slightly lower. The tropical ocean has large regions where the SST is high and relatively uniform, especially in the western Pacific and Indian Ocean regions. Much of the deep tropical convection occurs in this 'warm pool' region. The horizontal energy exchanges between the warm pool and other regions of the tropics are generally small ($\sim 35\ Wm^{-2}$) compared to the vertical exchanges of energy between the surface, the atmosphere and space ($\sim 300Wm^{-2}$), and so radiative-convective equilibrium (RCE) is a useful approximate model of the tropical and even the global climate (Manabe & Wetherald, 1967).

RCE can be studied with one-dimensional models, with limited-domain cloud-resolving models and with global general circulation models. High resolution models in a limited domain can be a means of studying the detailed physics of tropical convection and have revealed the tendency of convection to aggregate within a sufficiently large model domain (Bretherton et al., 2005; Cronin & Wing, 2017; Held et al., 1993; Tompkins, 2001a). RCE simulations have also been done with models in which the convection is parameterized (Held et al., 2007; Larson & Hartmann, 2003b,a). Investigating RCE in climate models with parameterized convection is done with several goals in mind (e.g. Wing et al. (2018)). One goal is to better understand how the parameterizations within the models perform in such simulations. In addition, more fundamental understanding of how the climate system works might be gained if it can be shown that the behaviors of in-

terest result from fundamental physical constraints that are not too dependent on the details of the parameterizations used in the models.

Simulations of RCE with global climate models (GCM) can be performed with fixed sea surface temperatures (SST) (Coppin & Bony, 2015; Held et al., 2007; Retsch et al., 2019) or with a slab ocean model, in which the SST interacts with atmospheric processes (Popke et al., 2013; Reed et al., 2015). In these simulations the convection aggregates in a portion of the model domain, in a fashion similar to cloud-resolving models. The self-aggregation process seems to be associated with a preference for convection to be located in regions that have already been moistened by convection, where radiative and microphysical interactions will favor convection (Bretherton et al., 2005; Tompkins, 2001b; Wing & Emanuel, 2014). Bony et al. (2016) argue that deep convective cloud fraction declines with SST due to increasing stability with decreasing pressure at cloud top, while Held & Soden (2006) argue that basic thermodynamic constraints require the convective mass flux to decline in a warming climate. Becker et al. (2017) have shown that convective aggregation in General Circulation Models (GCMs) is sensitive to the convective parameterization. GCMs with fixed SST have also been used to show the importance of cloud radiative effects on large-scale circulation (Harrop & Hartmann, 2015, 2016; Albern et al., 2018).

In a model with an interactive slab ocean, the ocean tends to be warm under the enhanced water vapor and cool elsewhere. This convection-SST interaction results in the organization becoming stronger and taking larger spatial and temporal scales. One particular case of interest is a "Tropic-World" simulation in which the planet does not rotate and the insolation is globally uniform. When done with a slab ocean model, these simulations typically develop large-scale persistent regions where SST is high and convection is common, and regions where SST is lower and convection is unlikely, much like the observed tropics (Popke et al., 2013; Reed et al., 2015). These simulations typically also have a limit cycle in which the SST contrast and the degree of aggregation oscillate at periods that depend on the mean SST and the depth of the mixed layer (Coppin & Bony, 2017).

In this paper we will consider Tropic-World simulations with the GFDL AM2.1 model with a slab ocean. We will focus primarily on the processes that determine the SST contrast in the equilibrated climate of the model in this paper. In Part 2 the mechanism of the oscillation will be investigated. In particular we wish to better understand the mechanisms whereby the SST, atmospheric circulation, evaporation and clouds interactively self-regulate. We will argue that these mechanisms are relevant to the observed tropical climate. Understanding the mechanisms that control the SST contrast within the Tropics is particularly important because it has been shown that the apparent sensitivity of climate is affected by the SST contrast. Zhou et al. (2016) showed with observations and modeling that SST pattern changes may have led to low cloud changes that suppressed global warming during recent decades. Dong et al. (2019) have shown in a modeling study that the change in SST over the western tropical Pacific warm pool is a key determinate of the net cloud feedback globally.

Coppin & Bony (2017) analyzed the variability in the LMDZ5A model run in Tropic-World mode. They found that for ocean layer depths greater than 10m, the model exhibits interannual variability. Their analysis indicates that the variability results from interactions among mean SST, SST gradients and convective aggregation. We find that the GFDL AM2.1 model generates similar variability, but here we are more concerned with the mean model climate and its sensitivity to warming. In addition, Coppin & Bony (2018) studied how the interplay between convective aggregation and SST gradients could impact equilibrium climate sensitivity (ECS). They found that convective aggregation in a fixed SST environment will reduce the ECS. When the SST is allowed to respond locally to heating, feedbacks associated with changing SST gradients between regions of ascent and descent act to offset this decrease in ECS. By analyzing how subsiding frac-

tion changes with temperature, they found that in the LMDZ5A model the SST pattern and gradients limit convective aggregation and its impact on the ECS.
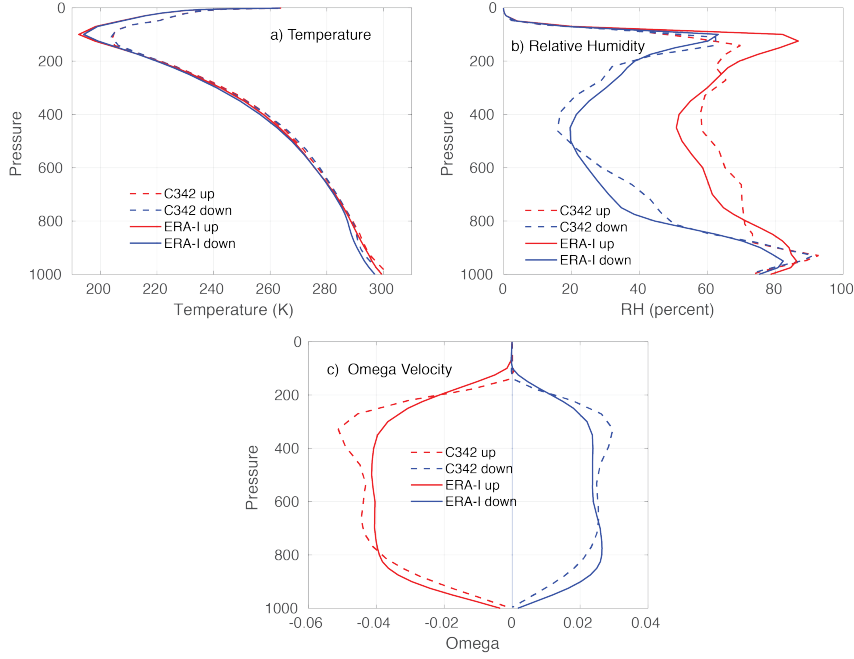
One of the interesting observations about the tropical climate is that the effects of tropical convective clouds on the top-of-atmosphere radiation budget tend to be small compared to large and opposing longwave and shortwave effects of clouds (D. L. Hartmann & Short, 1980; Ramanathan et al., 1989; D. L. Hartmann et al., 1992). GCMs in Tropic-World mode with slab ocean models have been used to study the role of two-way interactions of convection with SST in regulating SST variations and driving net cloud radiative effects toward neutral values (Wall et al., 2019).

In this study we will investigate the mechanisms that maintain the SST contrast in the equilibrated climate, and their sensitivity to warming. We find that as we warm the climate from one similar to the present-day tropics, the average SST contrast in the model increases, principally as a result of contrast in the longwave greenhouse effect in the rising and subsiding regions. Rising and subsiding are defined by the mass-averaged pressure velocity in monthly means. As the climate warms, the convective heating rate is shifted upward, becoming more top-heavy, leading to the production of more ice in the convective regions. We will show that these two results are simple consequences of radiative convective equilibrium and can be reproduced with a simple 1-D RCE model with fixed relative humidity and adjustment to a moist adiabatic lapse rate. For mean SST values between 300 and 309K the model is fairly insensitive to forcing, primarily because of the efficient longwave cooling in the subsiding region and because the net cloud response does not change the albedo as the climate warms. As the SST exceeds 310K the climate becomes much more sensitive because the greenhouse effect feedback in the subsiding region becomes stronger, while the greenhouse effect feedback in the region of upward motion becomes weaker. The shortwave cloud effect feedback always seems to try to reduce the SST contrast, and this effect also becomes stronger above 310K and helps to reduce the SST contrast at these warmer temperatures.

2 Model and Experimental Description

The model used is GFDL's CM2.1 Global Coupled Climate Model with a slab ocean model (Anderson et al., 2004; Delworth et al., 2006). The rotation rate is set to zero and the insolation is globally uniform. CO_2 is set to 324 ppm and CH_4 to 1650 ppb. Ozone is fixed to its tropical mean value. A horizontal spatial resolution of 2°latitude by 2.5°longitude, 32 vertical levels, and a time step of 900 seconds were used for the control experiments. Experiments were also conducted with 24 vertical levels and with increased horizontal resolution, and the basic behavior is the same. For our purposes, enhanced vertical resolution is important for resolving the upper troposphere and lower stratosphere. Held et al. (2007) examined the role of the column physics in fixed SST RCE experiments in CM2.0 and explored the transition from precipitation produced by the convection scheme to precipitation produced by grid cells approaching saturation, the so-called large-scale precipitation. This transition will be a significant factor in our experiments and has motivated comparing experiments of different horizontal grid spacing. Although resolution affects the behavior of the model in several ways, the basic mechanisms and conclusions presented here are robust to grid resolution changes of a factor of 2. It is likely that some model behavior is sensitive to the details of the cloud and convection parameterizations, so our conclusions should be tested with other climate models and cloud-resolving models, but that is beyond the scope of the present work.

A set of seven basic experiments were completed using a 50-meter slab ocean depth and incoming solar irradiance corresponding to the annual and diurnal averages at latitudes of 26°, 28°, 30°, 33°, 36°, 38°, and 45°: giving four hot climates, two climates corresponding to the current Tropics and a climate with the surface temperature of the current global average (Table 1). Each experiment was run long enough to produce 30 years
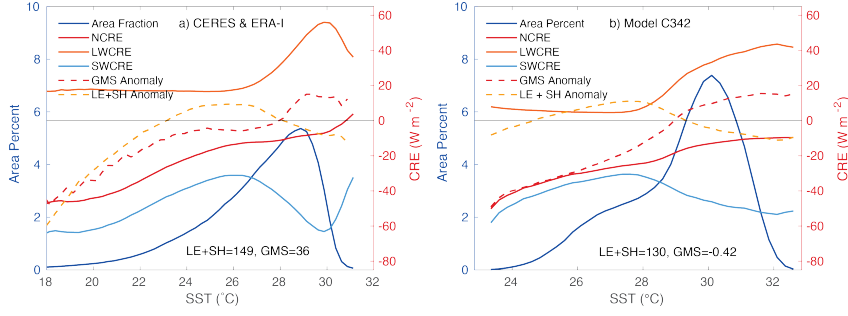
Figure 1. Comparison of a) Temperature, b) Relative humidity and c) vertical motion profiles versus pressure in regions of upward and downward motion for the average of monthly mean fields from ERA-Interim Reanalysis in the region within 22.5S to 22.5N and 90E to 270E, and the global average of monthly means for the C342 experiment, which has a global mean SST closest to the observed tropics. The relative humidity in both the model and the observations is determined by transitioning linearly from relative humidity above water to relative humidity above ice in the temperature range from 0 to -20°C

of stable climate for analysis after an initial spin up period that depends on the mixed-layer depth and starting climate. These experiments are denoted by their insolation and any additional modifications. For example, the control experiment with an insolation of 342 Wm^2 is called "C342." Experiments modified by doubling or quadrupling the CO_2 or using a 12-meter mixed layer depth are then called "C342-2x", "C342-4x", and "C342-12m" respectively

3 Comparison to Observed Tropics

In this section we explore how accurately Tropic-World emulates the observed Tropics for cases with similar SST to the current tropics, *e.g.* C342. Despite their simplifications, Tropic-World simulations have some basic characteristics in common with the observed tropics, so that we can argue they are a plausible analog to the observed tropics for our purposes. In particular, the vertical structure of temperature, relative humidity and mean vertical motion are important for what we want to investigate, and those very closely resemble the observed tropics.

To compare the model output to observations we use monthly SST data from NOAA OI interpolated data (Reynolds et al., 2007), radiation budget observations from CERES EBAF version 4 (Loeb et al., 2018), and atmospheric data and surface turbulent fluxes are from the ERA-Interim product (Dee et al., 2011). The period of overlap used is from March 2000 until October of 2018. Figure 1a shows that the temperature profile in the Tropic-World simulation is similar to that in the real tropics. The inversion in the sub-

Figure 2. Area fraction occupied by SST values, Cloud Radiative Effects (CRE), heating of the atmosphere by turbulent fluxes of latent and sensible heat at the surface (LE+SH), and vertically integrated export of energy by atmospheric motions (GMS). Turbulent fluxes and atmospheric export are plotted as anomalies from the area average over all SST values. a) CRE from CERES and energy fluxes ERA-Interim reanalysis for the region from the ocean regions between 22S-22N, b) the same quantities from the model run C342, which has a mean SST close to the observed Tropics of Earth.

siding region is stronger and closer to the surface in the model compared to observations, but the air temperature contrast in the boundary layer is smaller. The tropopause is warmer in the model, probably because the model does not have a Brewer-Dobson circulation in the stratosphere (Birner, 2010). The relative humidity distribution is similar to observations in the upward and downward regions to within 10%, but the model has a more uniform distribution of relative humidity in the region of rising motion, with larger humidity in the middle troposphere and lower humidity under the cold point in the region of rising motion. The lower humidity at the tropopause in the model may again have to do with the absence of a Brewer-Dobson Circulation. The vertical velocity structure in the upward and downward regions also agree with observations.

Figure 2 shows that the model has a similar negatively-skewed SST distribution as the real tropics, although the negative tail is not as long, likely because of upwelling regions within the tropical oceans. The longwave and shortwave cloud radiative effects (LWCRE and SWCRE) increase toward the warmest SST, but their sum, the net cloud radiative effect (NCRE) is much weaker and does not vary much within the warm pool. Over the warmest water the net cloud radiative effect is small, negative and almost independent of SST, although more negative than in the observations. The cloud radiative effects do not become smaller at the highest SST values as in the observations. This is likely because in observations the highest SST regions tend to occur where cloud and precipitation are consistently suppressed by large-scale circulations associated with fixed geographical features such as land and sea distributions, and those fixed constraints do not exist in Tropic-World. In Tropic-World high SST regions quickly attract convection and clouds, which cool the surface and suppresses the positive tail of the SST distribution.

Also shown on Figure 2 are the cooling of the surface by turbulent fluxes (LE+SH) and the net export of energy in the atmosphere (GMS). The turbulent cooling of the surface declines toward the maximum SST values, while the atmospheric energy export peaks at the warmest temperatures. The observed tropical atmosphere exports about 35 Wm^{-2} to the extratropics but the net atmospheric export of energy in Tropic World is zero. The export of energy from the warmest regions in Tropic World is about 20 Wm^{-2} and does not change much as the climate is warmed (not shown). Since its mean value is small and does not change much with warming it will not be discussed further in this paper.

It does seem to play a role in the oscillations about the mean state and will be discussed in a companion paper.

4 Mean Properties versus SST

In this section we describe the response of various global mean properties to global mean SST. Table 1 shows some climatological mean values for the seven control cases. The global albedo remains constant at about 22% for global mean SST between 302 and 309K, then declines for warmer SST values. Relative humidity declines slowly with warming, while subsiding fraction increases. Subsiding fraction is determined from the monthly and mass-averaged pressure velocity. Clear-sky atmospheric radiative heating rates are only slightly more negative than all-sky values. The difference in SST between regions of upward and downward motion at first increases, then decreases above 309K.
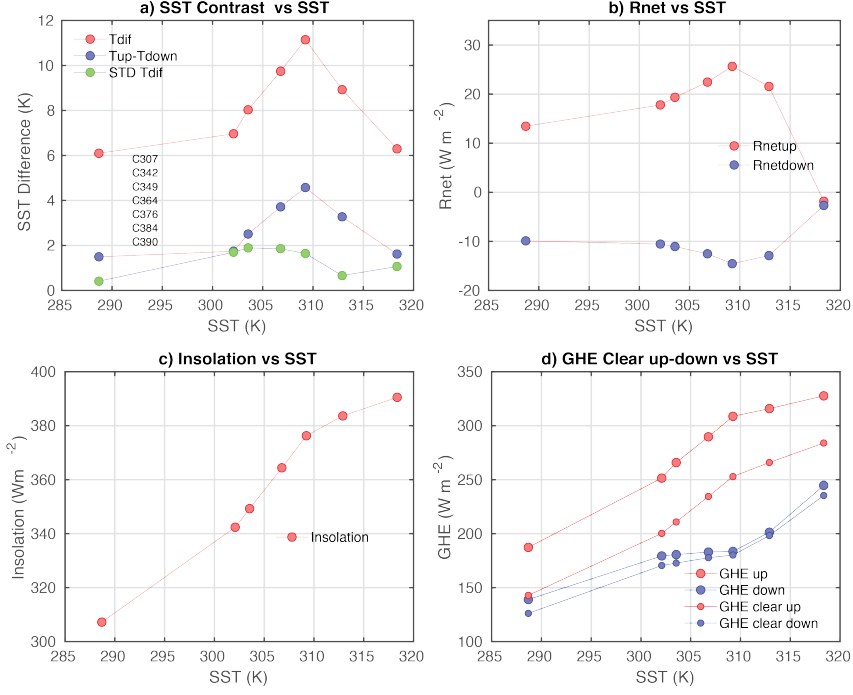
The model sensitivity can be calculated by taking the ratio of the mean SST change to the forcing for the C376 and C342 cases. Since the albedo remains constant at 22%, we can compute the forcing as the change in insolation multiplied by 0.78, the fraction of that change in insolation that is absorbed, giving a forcing of 26.45Wm^{-2}. The global mean SST change is 7.1K, so that the sensitivity parameter is 7.1K/(26.45Wm^{-2}) = 0.27 K/(Wm^{-2}), which means it would take almost 4Wm^{-2} of forcing to warm the SST by 1K. The primary reason for this insensitivity can be seen in Fig. 3d, which shows that the longwave greenhouse effect in the subsiding region barely increases at all from 302 to 309K. The longwave greenhouse effect is the difference between the upward longwave emission from the surface and the outgoing longwave radiation (OLR). Constant longwave greenhouse effect in the subsiding region means that the OLR increases there at approximately the rate that the blackbody emission from the surface increases. Part of the reason for this weak sensitivity is that the contrast between the free troposphere air temperature and the SST in the subsiding region increases with the difference in SST between the regions of upward and downward motion. The atmospheric temperature is controlled by the SST warming in the region of rising motion, while the SST warming in the subsiding area lags behind.

Case	Insol	SST	T_{dif}	Precp	SF	RH	OLR	Albedo	RHR	RHR$_{clr}$	T_{up}-T_{dn}
C307	307.2	288.7	6.1	2.8	0.58	48.9	234.7	0.24	-0.76	-0.81	1.5
C342	342.4	302.1	7.0	4.2	0.63	47.0	266.7	0.22	-1.02	-1.15	1.7
C349	349.3	303.5	8.0	4.5	0.65	46.0	271.5	0.22	-1.10	-1.24	2.5
C364	364.4	306.8	9.7	5.1	0.67	44.6	284.7	0.22	-1.28	-1.42	3.7
C376	376.3	309.2	11.1	5.6	0.67	43.6	295.1	0.22	-1.42	-1.56	4.6
C384	383.6	312.9	8.9	6.1	0.68	43.1	306.0	0.21	-1.55	-1.68	3.3
C390	390.5	318.4	6.3	6.4	0.75	42.8	317.3	0.19	-1.70	-1.85	1.6

Table 1. Insolation is in Wm^{-2}, Temperatures are in Kelvin, Precipitation is in mm day^{-1}, SF is subsiding fraction, RH is relative humidity in percent averaged over mass, RHR is radiative heating rate in Kday^{-1}, averaged over mass, RHRclr is the clear-sky value.

Figure 3a shows Tdif, the SST contrast for the top 20% of SST values minus the bottom 20% of SST values, as well as the difference between the SST in regions where the mass-averaged velocity is upward and downward. These differences increase for mean SST values between 302K and 309K, and then decline for larger mean SST values. The difference in net radiation also increases and then declines (Fig. 3b). Fig. 3c shows that the sensitivity of the global mean SST to insolation is small in the SST range of 302-309K, but then increases for warmer SSTs.

Figure 3. a) SST contrast as a function of mean SST, Tdif is the difference between the warmest and coldest 20% of SST values, Tup-Tdown is the SST difference between regions of upward and downward motion. The standard deviation with time of the monthly mean SST is also shown. b) the net radiation at the top of the atmosphere in the upward and downward regions, c) the insolation used in the experiment as a function of the global mean SST in equilibrium, d) the greenhouse effect in the upward and downward regions for both average and clear-sky conditions.

The greenhouse effect is the primary driver of the growth in SST contrast with warming (Figure 3d). The greenhouse effect grows by $50 \mathrm{Wm^{-2}}$ in upward region, but hardly at all in downward region. In the subsiding region the OLR increases at the same rate as the surface longwave emission, so that the greenhouse effect does not change with SST. In the upward region LWCRE, the difference between the clear-sky and all-sky OLR, stays almost constant, because the difference between the clear-sky emission temperature and the cloud top temperature remains constant, because both are tied to air temperature through the Clausius-Clapeyron dependence of saturation vapor pressure on temperature (D. Hartmann et al., 2019a). The clear-sky greenhouse effect (GHE) increases in the upward region. The difference between the upward and downward regions is because of the relative humidity (Fig. 1b), as discussed by Pierrehumbert (1995). The air temperature in the subsiding region is set by the SST in the region of rising motion in the Tropics (e.g. Fig. 1a) since the rotation rate is small. For this reason the emission temperature of the atmosphere can be warmer than one would expect from the mean SST, since the air temperature is not closely tied to the SST in the subsiding region. The SST contrast between the rising and sinking regions is thus a key parameter in climate sensitivity, and motivates the need for a deeper understanding of what controls this SST contrast. We see here that as this SST difference declines, the climate becomes more sensitive.

One can understand the greenhouse effect changes better by considering that the longwave GHE is defined here to be the difference between the longwave emission from the surface and the outgoing longwave radiation (OLR).

$$GHE = \sigma T_s^4 - OLR \tag{1}$$

Here σ is the Stefan-Boltzmann constant and T_s is the surface temperature. Start with the equation for the longwave cooling rate of the atmosphere as a function of the net longwave flux in the upward direction, F, where c_p is specific heat at constant pressure, ρ_{Air} is air density and z is altitude.
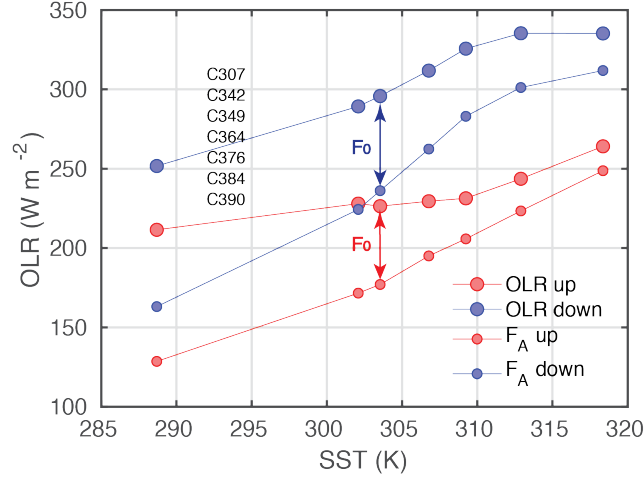
$$\frac{dT}{dt} = -\frac{1}{\rho_{Air}\,c_p}\frac{dF}{dz} \tag{2}$$

Integrating this equation though the mass of the atmosphere after using the hydrostatic relationship we obtain.

$$OLR = F(p_s) \; - \int_0^{p_s} c_p \frac{dT}{dt}\frac{dp}{g} \tag{3}$$

The OLR thus consists of two terms; the net longwave flux upward at the surface (F_0), plus the mass integral of the longwave radiative cooling rate (F_A). Figure 4 shows the OLR and the contribution to the OLR from the atmospheric cooling rate, F_A , for the upward and downward regions. The difference between OLR and F_A is the surface contribution F_0. In the region of rising motion, because the relative humidity is so high and clouds are present, the OLR does not increase very much in the range of temperatures between 300 and 310K. This is mostly because the net longwave loss at the surface is declining, primarily as a result of increased water vapor continuum absorption in the window region (e.g. D. Hartmann (2016), Fig. 10.10). The atmospheric cooling rate increases almost linearly with temperature across the entire range of SST values for reasons that we will explore subsequently by looking at the cooling rate as a function of pressure.

Figure 4 shows that in the region of subsiding motion the cooling rate of the atmosphere, F_A , increases more rapidly than in the region of upward motion, again principally because of the relative humidity distribution, but also because the air temperature is linked very closely to that in the region of rising motion, where it follows a moist adiabat tied to the near surface temperature. The net surface radiation loss decreases with increasing SST, but the emission from the atmosphere increases sufficiently fast to overcome this effect and give an OLR that increases at the same rate as the surface emission as shown in Figure 3d. The insensitivity of the clear-sky greenhouse effect in the
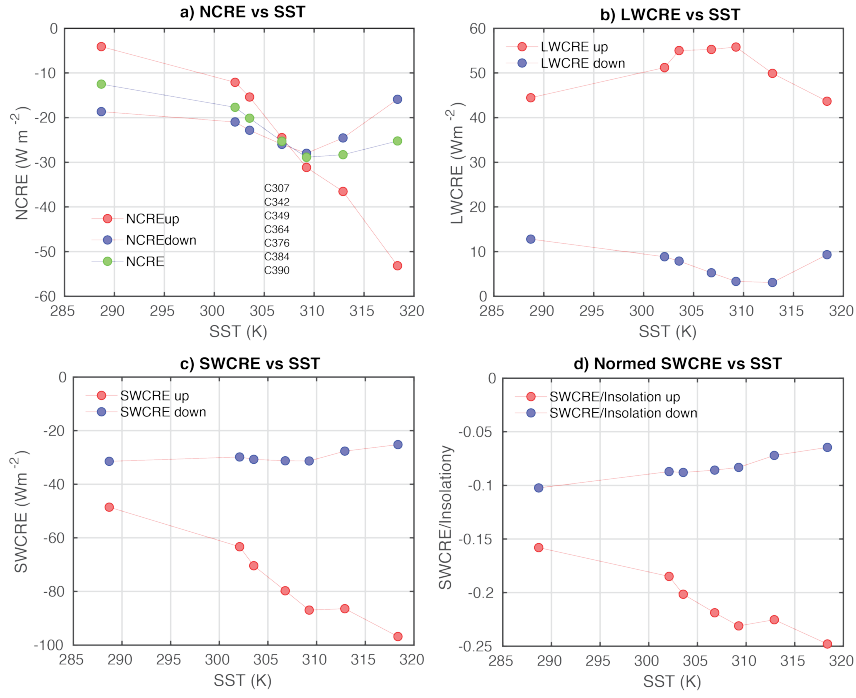
Figure 4. OLR and atmospheric cooling rate contribution to OLR from F_A and F_0 in the upward and downward regions as a function of global mean SST for the seven basic experiments. F_0 is the difference between OLR and F_A, as indicated by the arrows for case C349.
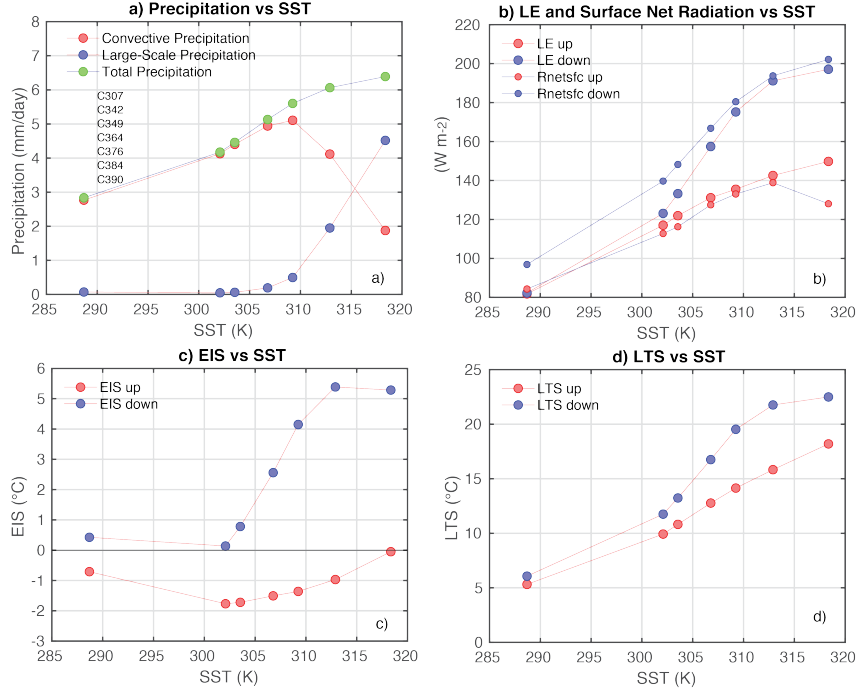
subsiding region to mean warming depends strongly on Tdif, the SST contrast parameter, since the atmospheric emission temperature in the subsiding region is tied to the warmer SST in the rising region. Motions quickly respond to redistribute mass to decrease pressure gradients. This dynamic balance also explains why the air temperature above the boundary layer in the subsiding region is slightly warmer than the air temperature in the rising region, when the air temperature below the inversion is colder in the subsiding region (Fig. 1a).

Above mean SST of 310K, the surface longwave loss, F_0, reaches a limiting value and the OLR must follow the linearly increasing F_A. This increases the local climate stability in the warm region. In the subsiding region the OLR stops increasing above 310K because the surface longwave loss declines, but also because the atmospheric cooling rate begins increasing much more slowly with increasing SST. One may ask why the atmospheric emission can continue to increase in the rising region, whereas its increase with SST begins to slow in the subsiding region. The explanation for this seems to reside in the differing responses of longwave radiative cooling of the atmosphere in the rising and subsiding regions, which will be discussed in Section 5

The cloud radiative effects are also of importance. Fig. 5a shows that net cloud radiative effect (NCRE) in the region of upward motion becomes more negative by about $20\mathrm{Wm}^{-2}$ between 302 and 309K, while Fig. 3d shows that the GHE becomes more positive by about $50\mathrm{Wm}^{-2}$. We thus conclude that the increased cloud shading is acting to suppress the warming in the upward region, but it is overwhelmed by the increases in the clear-sky GHE there, causing the SST to warm more rapidly in the upward region. Beyond 309K the SWCRE in the upward region continues to become more negative, almost linearly between 302K and 318K. The NCRE in the subsiding region does not change as much as in the rising region. Because the insolation is being increased to warm the model, it is instructive to normalize the SWCRE by the insolation, so that it forms the negative of the albedo enhancement by clouds. This is shown in Fig. 5d. The normalized SWCRE in the subsiding region becomes slightly more positive as the climate is warmed, especially for SSTs greater than 309K. In contrast, the normalized SWCRE in the upward region becomes more negative with SST and by a larger amount. The SWCRE changes are thus working to reduce the SST contrast, while the greenhouse effect is re-

Figure 5. a) Net Cloud Radiative Effect (NCRE) for upward, downward and global mean averages, b) Longwave Net Cloud Radiative Effect (LWCRE) vs SST for upward and downward regions, c) Shortwave Cloud Radiative Effect (SWCRE)for upward and downward regions and d) SWCRE divided by insolation for upward and downward regions all as functions of global mean SST.
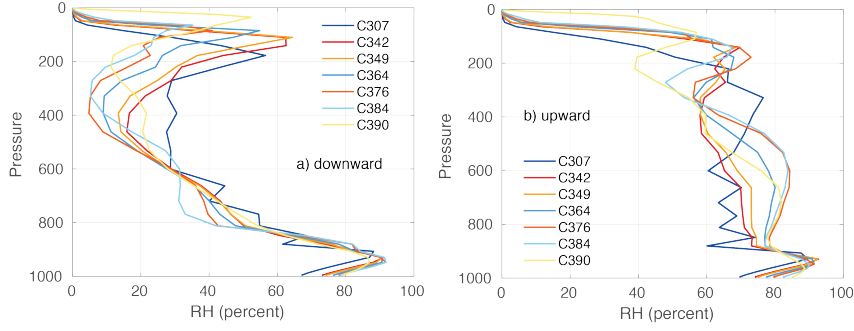
Figure 6. a) Precipitation, b) Surface evaporative cooling rate (LE) and Surface net radiative flux, c) Estimated inversion strength (EIS) and d) Lower Tropospheric Stability (LTS) as functions of SST for the seven control experiments.
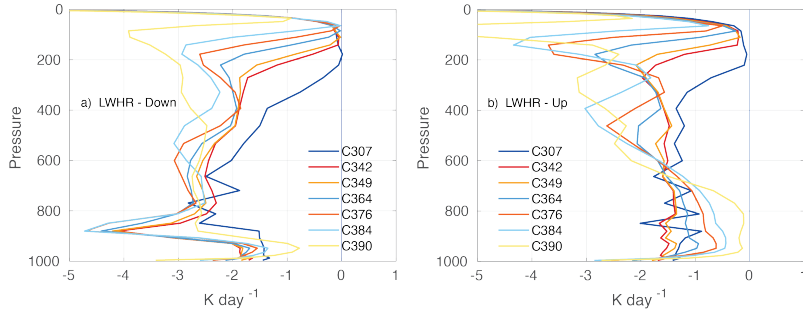
sponsible for the increase in SST contrast. The atmospheric transport from the rising region to the subsiding region is relatively small and does not change very much as the climate is warmed (Supplementary materials).

We thus conclude that the SST contrast increases with temperature as the SST is increased above present values because the clear-sky greenhouse effect increases rapidly over the warm, moist region, while in the subsiding region the OLR increases almost as fast as the surface longwave emission does. Cloud shortwave effects in the region of rising motion act to offset the increasing greenhouse effect in the warm region, but are smaller than the increases in longwave greenhouse effect. In the subsiding region the low cloud albedo is relatively insensitive to SST increases and does not appear to play a key role in constraining the SST contrast.

Figure 6a shows the convective, large-scale and total precipitation rates as a function of SST for the control experiments. Above 310K the large-scale scheme produces increasing fractions of the total precipitation. The transition to large-scale precipitation is somewhat resolution-dependent and occurs at lower SSTs if the model resolution is increased from 2-degrees to 1-degree (not shown). Figure 6b shows that the evaporative cooling rate closely follows the net radiative heating of the surface, since the sensible cooling and heat storage are both small. The inversion strength, whether measured by Estimated Inversion Strength (EIS, Wood & Bretherton (2006)) or Lower Tropospheric Stability (LTS, Klein & Hartmann (1993)) increases particularly strongly across the range of temperatures from 300 to 310K (Figures 6c,d).

Figure 7. Relative humidity in the a) downward and b) upward regions as functions of air pressure for the seven basic experiments.

Figure 8. Longwave radiative cooling rate in the a) downward and b) upward regions for the seven basic experiments. (the total radiative heating rate shows similar structural changes)

5 Vertical Structure of Humidity and Heating Rate

We next show that the vertical distribution of relative humidity in the upward and downward regions changes modestly with warming SST, and we show that the mass-integrated atmospheric cooling rate increases by extending upward, rather than by increasing at each pressure level. Figure 7 shows the relative humidity in the downward and upward regions for the basic set of experiments. It was previously shown in Figure 1 that the relative humidity in the upward and down regions of the model is in qualitative agreement with ERA-Interim data for the tropics. The relative humidity peaks at the top of the boundary layer at about 90% in both the upward and downward regions. In the downward region the relative humidity decreases above the boundary layer approximately linearly in pressure up to a minimum of less than 20% at around 400-300hPa, depending on the surface temperature. It then increases up to the top of the troposphere where it reaches a secondary maximum of about 50%. In the region of rising motion the relative humidity remains higher at between 60 and 80% all the way to the tropopause region. These differences are very significant for the greenhouse effect of water vapor (Figure 3d). Between SST values of 300K and 310K the model shows a tendency for the upper troposphere to become drier in the subsiding region and for the relative humidity in the lower free troposphere to become higher with SST. Beyond 310K the character of the model solution changes, and these tendencies are reversed to some extent.

Fig. 8 shows the atmospheric longwave cooling rate as a function of pressure for the seven basic experiments. This plot includes cloud effects, but is not greatly different from the clear-sky plot. In both the downward and upward regions, the mass-integrated cooling rate, which is related to the OLR (Equation 3), increases by extending upward

more than by increasing uniformly. In fact, in the lowest troposphere the cooling rate generally weakens with increasing SST. This is especially true in the upward region, where the cooling rate in the lower troposphere weakens with increasing SST over a deep layer. For the warmest cases the radiative cooling rate in the lower troposphere becomes quite small as the atmospheric column approaches a decoupled state that would lead to a runaway greenhouse effect, if the whole troposphere was as moist as the upward region (Renno, Emanuel, & Stone, 1994; Renno, Stone, & Emanuel, 1994). The importance of the dry, subsiding region for stabilizing the climate was described by Pierrehumbert (1995).
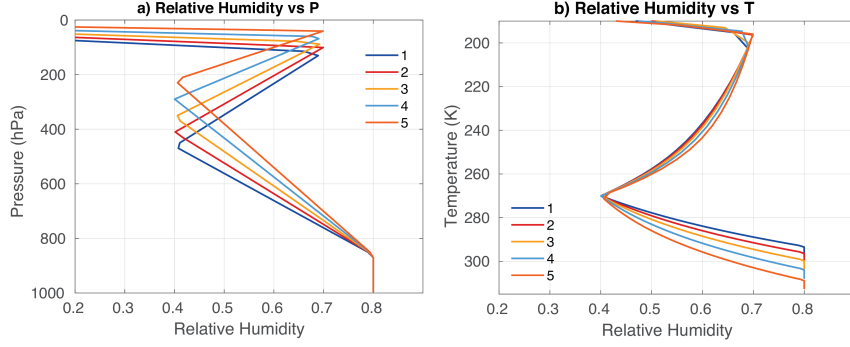
We return here briefly to the question of why the OLR in the subsiding region has a weaker dependence on surface temperature for the very warm climates (Figure 4). Figure 8 indicates that in the rising region where relative humidity is high in the free troposphere, the cooling rate starts out low, but increases fractionally faster in the upper troposphere. In the subsiding region, however, the radiative cooling starts out higher, but the increases in cooling at the top that drive OLR increases in warm climates are less effective, and at very warm temperatures the increases in cooling at the top are less able to compensate for decreases lower down. This is because of the extremely low relative humidity in the upper troposphere of the subsiding region, which is less than 10% over a deep layer for the warmest cases (Figure 7). In the subsiding region the radiative cooling from the lower troposphere begins to saturate at high temperatures, but the dry upper troposphere cannot compensate for this by extending the cooling upward because of the low humidity there.

5.1 1-D RCE Experiments

The upward extension and increase of the cooling rate are a consequence of the nearly moist adiabatic lapse rate and the dependence of water vapor saturation on temperature. This can be demonstrated with a simple one-dimensional radiative-convective equilibrium model. We follow the same adjustment procedure as Manabe & Wetherald (1967), except that the lapse rate relaxes to a moist adiabatic lapse rate with a one-hour time scale. The radiation code is RRTMG (Mlawer et al., 1997; Clough et al., 2005). The model experiments here and interpretation of some convection-resolving experiments by Romps (2014), suggest that the upper-tropospheric relative humidity is nearly a fixed function of temperature. To approximately fit the observed mean profile of relative humidity we use a piece wise linear function of pressure, which is a constant 80% below 850 hPa, declines linearly to a minimum of 40% at the pressure where the temperature is 270K, then increase to 70% where the radiative cooling rate falls to -0.2 Kday^{-1}, then decline linearly to a stratospheric value at a pressure that is half of the value where the upper relative humidity peak occurs. This distribution is a reasonable fit to the relative humidity distribution shown in Figure 1b. To be consistent with the GCM and ERA Interim reanalysis, we assume that the saturation vapor pressure transitions linearly from that of liquid at 273K to ice at 253K. As the climate is warmed, the mid-tropospheric minimum and the upper tropospheric maximum in relative humidity tend to maintain a constant temperature as they move to lower pressures. The tendency of the required convective heating rate profile to become more top heavy with increasing surface temperature can be illustrated well enough with a model that has uniform relative humidity, but we introduce this more complicated profile for use later.

The CO_2 is set to 300ppm, other trace gases are present in their current abundances and the surface albedo is set to 10%. The temperature is varied by changing the insolation, as in our GCM experiments, but to get SST values in the range desired, different insolations need to be used depending on the relative humidity profile and whether ozone is included or not.

Figure 9 shows the humidity profiles from the solution to the 1-D RCE computations with no ozone. The pressure of the mid-tropospheric minimum follows a fixed tem-

Figure 9. Relative humidity as functions of a) pressure and b) temperature that result from the 1-D RCE calculations shown in Figure 10

perature of 270K, while the upper maximum follows the level where the radiative cooling rate falls below -0.2K/day, which is very close to the level where the cooling rate goes to zero at the top of the convecting layer. The results are not very sensitive to this choice of -0.2K/day, but since there is no convective overshoot or Brewer-Dobson circulation to support a transition to radiative warming above the top of the convecting layer in this 1-D model, it is felt that a small negative cooling rate threshold would be more robust for computational purposes than zero radiative cooling rate. The five cases represent different surface temperature values that were induced by changing the insolation.
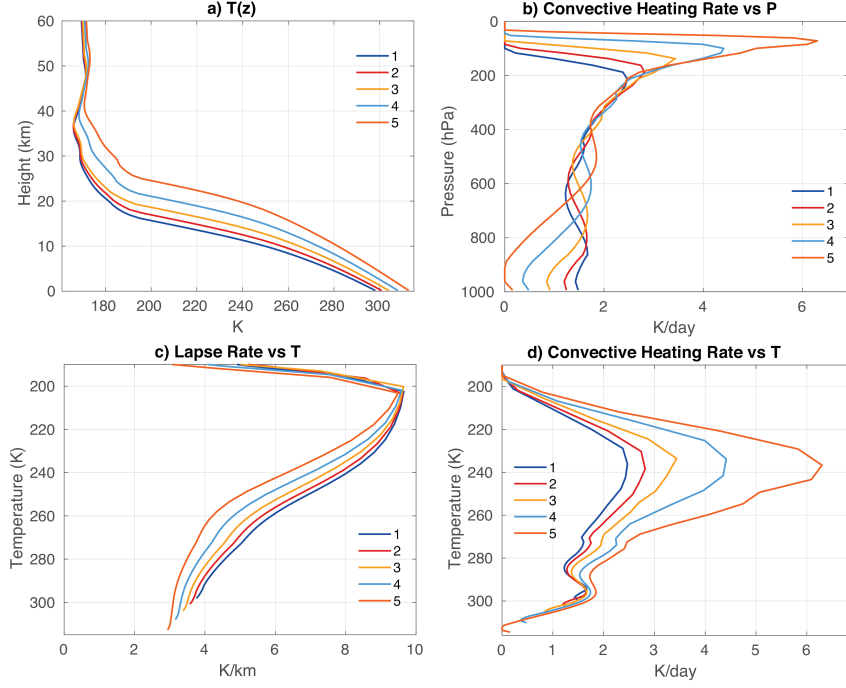
Figure 10 shows the results of RCE computations with zero ozone and the relative humidity profiles shown in Figure 9. The temperature profile follows a moist adiabat up to about 200K where it approaches the dry adiabatic lapse rate before becoming abruptly more stable at colder temperatures above that level. This lapse rate kink occurs at very nearly the same air temperature and same lapse rate value as the surface temperature is varied across a wide range, as expected given the dependence of water vapor on temperature alone and strengths of the rotational emission lines of water vapor (D. L. Hartmann & Larson, 2002; Jeevanjee & Fueglistaler, 2020b). The minimum dry stability shows no pressure dependence, and always approaches the dry adiabatic value at the top of the convecting layer. Below that the stability throughout the troposphere is increased because of the assumption of a moist adiabatic temperature profile. While the dry adiabatic lapse rate is independent of pressure, the moist adiabatic lapse rate depends on pressure through the dependence of saturation specific humidity on pressure at a fixed temperature.

The convective heating rate, which is equal and opposite to the radiative cooling rate, becomes more top heavy in pressure space (Figure 10b). In temperature space the cooling rate profile stays at about the same temperature, but increases in magnitude. The supplementary materials show a similar plot for the case in which the ozone concentration is set to the observed tropical profile as a fixed function of pressure. In that case the lapse rate change occurs at about 220K, 20K warmer than the no-ozone case, and is more sensitive to warming (Harrop & Hartmann, 2012).

5.2 Theoretical Explanation for the Top-heavy Radiative Cooling Profile

The increase in magnitude of the radiative cooling rate with surface temperature can be understood theoretically by using the cooling to space approximation (Rodgers & Walshaw, 1966; Petty, 2006; Jeevanjee & Fueglistaler, 2020a). Begin with the cooling-to-space approximation for the water vapor radiative heating rate at a particular wave-

Figure 10. 1-D RCE results for a cases with no ozone and the relative humidity profiles shown in 9. a) Temperature as a function of altitude, b) convective heating rate as a function of pressure, c) lapse rate as a function of air temperature and d) convective heating rate as a function of air temperature.

length, λ.

$$\left.\frac{dT}{dt}\right)_\lambda = -\frac{\pi \, k_\lambda \, \rho_{H_2O}}{\rho_{Air} \, c_p \, \bar{\mu}} \, B_\lambda(T) \, e^{\frac{-\tau_\lambda}{\bar{\mu}}} \tag{4}$$

Here $\bar{\mu} = 1.66^{-1}$ is the average over a hemisphere of $\mu = cos\theta$, k_λ is the mass absorption coefficient and τ_λ is the normal optical depth from the given height to the top of the atmosphere. Next use the following identity

$$\frac{\rho_{H_2O}}{\rho_{Air}} = 0.622 \, RH \, \frac{e_s}{p}. \tag{5}$$

Here RH represents relative humidity and e_s is the saturation vapor pressure. And from the work of Chou et al. (1993) we assume a linear dependence of the mass absorption coefficient on pressure.
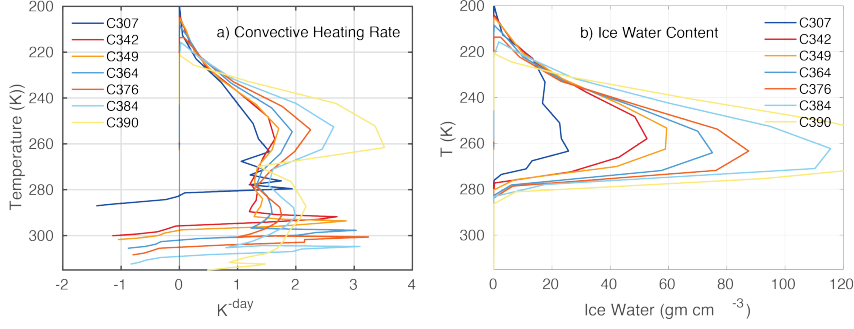
$$k_\lambda = k_{\lambda 0} \frac{p}{p_0} \tag{6}$$

So we find that,

$$\left.\frac{dT}{dt}\right)_\lambda = -\frac{0.622 \, \pi}{c_p \, p_0 \, \bar{\mu}} \, e_s(T) \, RH \, k_{\lambda 0} \, B_\lambda(T) \, e^{\frac{-\tau_\lambda}{\bar{\mu}}}. \tag{7}$$

We write the optical depth using the hydrostatic approximation as,

$$\begin{aligned}
\tau_\lambda &= \int_z^\infty k_\lambda \, \rho_{H_2O} \, dz = \int_0^p k_{\lambda 0} \, \frac{p}{p_0} \, 0.622 \, \frac{e_s}{p} \, RH \, \rho_{Air} \, \frac{dp}{g \, \rho_{Air}} \\
&= \frac{k_{\lambda 0} \, 0.622}{g \, p_0} \int_0^p RH \, e_s(T) \, dp = \frac{k_{\lambda 0} \, 0.622}{g \, p_0} \, \overline{RH \, e_s(T)} \, p
\end{aligned} \tag{8}$$

Figure 11. a) Globally averaged total convective heating rate and b) ice concentration as functions of air temperature for the control experiments with AM2.1.

So the final form that we can write is,

$$\frac{dT}{dt}\Big)_\lambda = -\frac{0.622\,\pi}{c_p\,p_0\,\bar{\mu}}\,e_s(T)\,RH\,k_{\lambda 0}\,B_\lambda(T)\,e^{(-C\,k_{\lambda 0}\,\overline{RH\,e_s(T)}\,p)}. \tag{9}$$
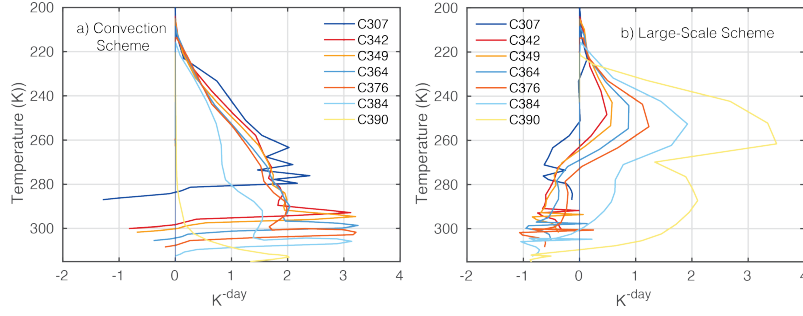
Where C is a constant.

$$C = \frac{0.622}{p_0\,g\,\bar{\mu}} \tag{10}$$

In equation (9) the only pressure dependence is in the optical depth, all the other terms depend only on temperature. Next we assume, following the Fixed Anvil Temperature (FAT) theory (D. L. Hartmann & Larson, 2002) that the clear-sky cooling rate profile is approximately fixed as a function of air temperature. Then the saturation vapor pressure and the Planck emission are also fixed as functions of temperature. So the only term in equation (9) that is likely to change under FAT is the final exponential, which will get larger as the surface warms and the cooling rate moves higher in the atmosphere, while maintaining a constant temperature. In the control experiments the level where the cooling rate peaks moves from 200hPa to 100hPa as the climate warms so the exponent in the transmission term in equation (9) varies by a factor of 2.

5.3 Implications of Radiative Cooling for Cloud Ice

It is important for ice formation that the cooling rate increases most where the air temperature is below freezing. This is shown for the GCM results in Figure 11a. More cooling means more active convection, which will likely mean more ice production and greater average ice concentration. This expectation is confirmed in Figure 11b. The increasing ice content is consistent with the increasing reflectivity of the region of rising motion in Figure 5.

An important consequence of the radiative cooling rate and convective heating rate becoming more top-heavy with increasing SST is that the GCM's parameterizations have to be able to adjust to provide this different heating structure as the climate warms. This is achieved in the GCM used here by increasing the amount of precipitation that is produced by the large-scale scheme as opposed to the convection scheme. The large-scale precipitation is sometimes also referred to as stratiform precipitation. Held et al. (2007) have noted how the GFDL AM2.1 model we are using here produces more grid-scale convection via the large-scale scheme as the SST warms. Figure 12 shows the vertical structure of the convective and large-scale heating rates as functions of air temperature. The increase in convective heating rate in the upper troposphere peaking around temperatures of 250K is contributed almost entirely by the large-scale scheme. The convective scheme seems only able to produce a convective heating rate that declines upward. The
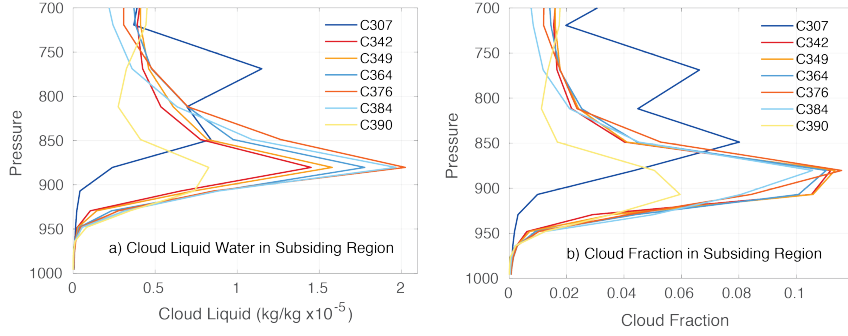
Figure 12. Convective heating rate plotted versus air temperature for the a) convection scheme and the large-scale scheme for the control experiments with AM2.1.

increasing importance of the large-scale scheme can thus be regarded as the model's response to the requirement that the convective heating balance an increasingly top-heavy radiative cooling profile. One can also see that for the warmest temperatures the convection scheme contributes less as the atmosphere approaches its runaway greenhouse condition.

5.4 Low Cloud Response

We next turn to the very modest changes in cloud reflectivity in the region of subsiding motion. Why does the SWCRE seem to decline a little over the subsiding region with increasing temperature as the SST warms from present values and the SST contrast also increases? Figures 6c,d indicate that the estimated inversion strength (EIS, Wood & Bretherton (2006)) and lower tropospheric stability (LTS, Klein & Hartmann (1993)) both increase in the subsiding region as the climate is warmed above present values. The dynamic forcing associated with enhanced stability would be expected to increase the low cloud fraction and albedo. Figure 13 shows that the cloud fraction stays about constant, and liquid water content increases only slightly in the boundary layer of the subsiding region between C342 (302K) and C376 (309K), but then declines for the warmest cases C384 (313K) and C390 (318K). The cloud fraction is approximately constant, until it decreases for SST greater than 310K. The low clouds thus thicken slightly between 302 and 309K mean SST and this would increase the reflectivity of the low clouds. The effect of this increased cloud albedo is offset by the increased absorption of solar radiation in the atmosphere by water vapor as the SST increases, because the amount of water vapor in the atmosphere increases a lot. The insolation is also increasing, but the effect of this is minor compared to the large increases in water vapor abundance with temperature. The effect of the enhanced shortwave absorption by water vapor is discussed in the supplementary material.

In the region of subsiding motion, the lower tropospheric stability (LTS) and the estimated inversion strength (EIS) both increase. All else being equal one would expect the dynamical effect of the increased inversion strength to increase the low cloud fraction and albedo in the subsiding region (Klein & Hartmann, 1993; Wood & Bretherton, 2006; Bretherton, 2015)). As the climate warms, however, the vertical gradient of specific humidity in the lower troposphere increases very rapidly with SST. This would be expected to decrease the cloud amount through thermodynamic mechanism discussed by Bretherton & Blossey (2014) that is related to the increased vertical gradient of moisture in warmed climates (Brient & Bony, 2013). It appears that the dynamic and thermodynamic mechanisms approximately cancel each other in this model, such that the net change in the low cloud radiative effect in the subsiding region is small across a large range of SST. Sherwood et al. (2014) show that the low cloud feedback varies a lot across

Figure 13. a) Cloud liquid water content (LWC) and fraction and b) cloud fraction below 700hPa in the region of subsiding motion. The LWC increases up to the case C376, then declines. The cloud fraction remains approximately constant up to case C376, after which it declines in a transition in which the SST difference is reduced with warming.

models in large measure because of differences in the way the thermodynamic effect of increased specific humidity gradients on low clouds is modeled. The collapse of the low clouds at the highest temperature is somewhat like the low cloud catastrophe envisioned by Schneider et al. (2019), but by this point the region of upward motion is also reaching an extreme, nearly decoupled state.
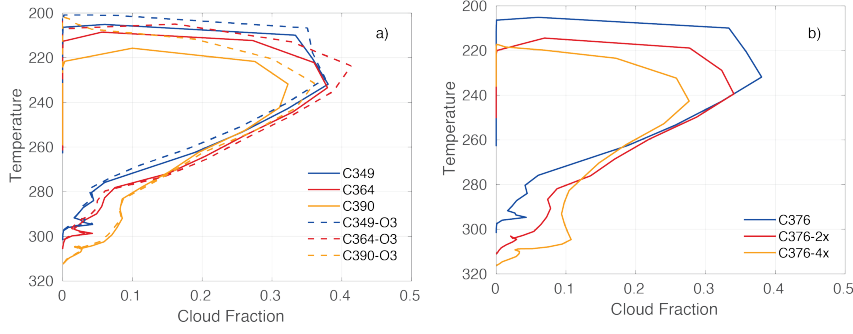
6 Sensitivity Studies

6.1 Insolation versus CO_2 Forcing

In these experiments we have varied the global mean SST by changing the insolation. The question arises whether the method of forcing the warming matters, or whether the behaviors we highlight here result from basic moist thermodynamic considerations and are nearly independent of the method of forcing. To explore this across the full range of SST we have done additional experiments in which we fix the insolation, then double or quadruple the CO_2 to produce additional warming. These experiments indicate that the basic response to SST in Tropic-World does not depend sensitively on the method of forcing, but mostly depends on the SST, which sets the moist thermodynamics and dominates the model response. In the supplementary material we show that the key responses of the model to SST changes are similar whether the SST changes are forced with insolation or with CO_2. The greenhouse effect in the subsiding region increases when CO_2 is added, compared to a case in which the SST is the same but the CO_2 is not increased. For higher temperatures this effect is generally smaller, because the greenhouse effect is more completely dominated by water vapor. The faster warming in the region of upward motion than downward motion is not affected. Subsiding fraction, relative humidity and albedo are strictly functions of SST and are not affected by the presence of CO_2 except through the additional surface warming that it produces.

6.2 Ocean Heat Capacity

The experiments shown so far have all been done with a 50-meter slab ocean model. We repeated some of the experiments with a 12-meter slab ocean model, and, although the climate is slightly different, the basic model behaviors highlighted in this paper are reproduced.

Figure 14. Cloud fraction plotted against temperature as the vertical coordinate. a) cases C349, C364 and C390 with tropical ozone profile (solid), and cases with the same mean SST, but with tropical ozone times 10^{-6} (dashed). b) for case C376 but with 1X, 2X and 4X CO_2 concentration and tropical ozone.

6.3 Stratospheric Ozone

Harrop & Hartmann (2012) performed experiments with a cloud resolving model to show that ozone heating could cause cloud tops to warm as the SST is increased, because warming raises the clouds to regions where ozone heating becomes important if ozone is specified as a fixed function of pressure. In an atmosphere whose only radiatively active gas is water vapor, the model cloud tops remained at the same temperature as the SST was increased, in agreement with the FAT theory (D. L. Hartmann & Larson, 2002). We performed experiments in Tropic-World in which we reduced the ozone to a small value. Because of the important greenhouse effect of ozone, however, this causes the climate to cool, so in addition we did another set of experiments in which the ozone was reduced, but the global mean SST was maintained at the same value as in the control experiment by applying a small heating to the slab ocean model at every location. Figure 14a shows that the presence of ozone causes the top edge of the cloud to be around 10K warmer, especially for the warmest cases. The sensitivity of the cloud top temperature to surface temperature is also increased when ozone is incuded. Figure 14b shows that the decrease in cloud fraction and increase of cloud top temperature also occurs when the climate is warmed with CO_2 when ozone is fixed.

6.4 Relative Humidity

Figure 14 indicates that ozone contributes significantly to the warming of cloud top and reduction of cloud fraction when the surface warms and forces convection upward into the region where ozone heating is more substantial and causes a reduction in lapse rate. This is different from the results of Bony et al. (2016), who stated that their reduction in cloud fraction was not dependent on ozone and argued for a mechanism involving the dependence of static stability on pressure. In our experiments ozone is important, but even with small ozone values the cloud top temperature increases with surface warming. Zelinka & Hartmann (2010) and Bony et al. (2016), have suggested that the warming and suppression of cloud fraction with warming results from a pressure effect on static stability. If the top of the convecting layer is sufficiently cold, the lapse rate should approach the dry adiabatic if convection is balanced by emission from water vapor, as shown in Figure 10c and in cloud-resolving simulations in which water vapor is the only radiatively active gas (Harrop & Hartmann, 2012; D. Hartmann et al., 2019a). The moist lapse rate where the saturation vapor pressure is higher does have a dependence on pressure as well as temperature, however, because the saturation specific humidity at a fixed temperature increases with decreasing pressure. With this in mind we

offer an alternative explanation for why the cloud tops get slightly warmer even when ozone is not present. For the Tropic-World simulations, one possible reason could be that the relative humidity near the top of the troposphere decreases with surface warming (Figure 7). From equation (9) we see that the relative humidity enters both in the emission and the transmission parts of the cooling to space approximation. If the RH decreases with warming, the clear-sky radiative cooling will weaken with it. This will shift the peak of the radiatively-driven divergence downward to warmer temperatures and cause the cloud top temperature to warm. Thus from the basic FAT theory mechanism we expect that the cooling from water vapor will weaken at a fixed temperature if the relative humidity is reduced in the upper troposphere (Harrop & Hartmann, 2012) and that this will lead to warming of the cloud top temperature.

To test the role of the relative humidity on cooling rate in the upper troposphere of the subsiding region we undertake some additional RCE experiments with our one-dimensional model. To simply model the relative humidity changes in Figure 7 we adjust the value of the relative humidity maximum at the top of the convecting layer. In the supplementary materials we show that reducing the peak relative humidity at the top of the convecting layer from 80% to 40% makes the temperature of the upper convective heating maximum warmer by 5K. This is about half of the warming of cloud top see in Figure 14a, but much smaller than the 20K warming associated with fixed ozone. Equation (9) indicates that the relative humidity enters in two places in determining the cooling rate. The emission is linear in the relative humidity, and so should decrease substantially, but the lower relative humidity also means that the transmission of that radiation to space will become more efficient with lower relative humidity, so these two effects partially cancel. Cloud resolving model simulations (Kuang & Bretherton, 2004; D. Hartmann et al., 2019b) and simulations with single column convective parameterizations (D. L. Hartmann & Berry, 2017) indicate that convective overshoot is important near the top of the convective layer, which may make the rate of destabilization below the level of neutral buoyancy important for the cloud fraction at cloud top. Thus in a more realistic simulation we might expect the average cloud top position to be more sensitive to the radiative destabilization rate immediately below the level of neutral buoyancy than in our 1-D simulation. In that case drying out of the upper troposphere with warming may provide a plausible mechanism for the warming of cloud tops and the decrease in high cloud fraction in the Tropic-World simulations shown here.

7 Conclusion

We have investigated the processes that determine the mean sea surface temperature contrast in a climate model run in Tropic-World mode, with no rotation, uniform insolation and a slab ocean model. The mean SST difference between regions of rising and subsiding motion increases as the climate is warmed above mean SST values comparable to today's. This increase in SST contrast occurs because the clear-sky greenhouse effect increases more rapidly for the moist atmosphere overlying the region of upward motion and high SST values than for the drier subsiding region with cooler SSTs.

In the particular model used here the global mean albedo does not change much with SST. The albedo decreases slightly with mean SST in the subsiding region where low clouds are present and increases steadily in the region of upward motion and deep convection. The low-cloud albedo in the subsiding region does not change much with SST, apparently because as the climate is warmed, increases in estimated inversion strength, which should increase low cloud albedo, are offset by thermodynamic processes, which provide more drying of the boundary layer by entrainment of air from above as the SST is increased.

High clouds in the region of upward motion and deep convection become more reflective and increase their ice content with warming. This occurs because the strength

of radiative destabilization in the air temperature regime where ice clouds form is strengthened with warming. As the SST is warmed the radiative cooling rate of the atmosphere strengthens by extending higher and increasing in magnitude, while the cooling rate in the lower troposphere remains approximately constant or declines. This can be understood as a purely clear-sky radiative effect by considering a one-dimensional radiative-convective equilibrium model, and using the cooling to space approximation as a guide. One can then conclude that the amount of ice in the tropical atmosphere should increase with warming, if the ice amount is proportional to the radiative cooling rate in the atmospheric layers where ice is formed. The increasingly top-heavy structure of the radiative cooling profile may be a partial explanation for why the precipitation in the model shifts progressively from the convection scheme to the large-scale scheme as the climate warms. The convection scheme produces a bottom-heavy convective heating profile at all SST values.

As the mean SST approaches 310K and the temperature in the region of rising motion approaches 315K, the SST difference begins to decline with warming and the climate of the model becomes more sensitive to further positive climate forcing. Below 310K the efficient cooling from the region of subsiding motion keeps the Tropic-World climate relatively insensitive, warming only about 0.26K for each Wm^{-2} of forcing. In the region of subsiding motion, the greenhouse effect feedback is nearly absent and the OLR increases at almost the rate that would be predicted from the Planck emission of the surface temperature.

Very strong positive feedbacks are engaged as the SST contrast begins to decline, which both lead to further decreases of the SST contrast and a more unstable global climate. Much of the reason for this sudden change appears to originate in the increasing amount of water vapor in the lower atmosphere. In the subsiding region the OLR begins to increase more slowly with SST above 310K, because the emission from the atmosphere becomes less sensitive to SST, while the contribution from surface emission also declines. In the region of rising motion, the contribution of surface emission to OLR reaches a limiting minimum value, while the emission from the atmosphere continues to increase approximately linearly with SST, so that the sensitivity of OLR to SST increases above 310K. As the SST contrast declines in response to changes in the longwave radiative feedbacks in the rising and subsiding regions, the reduction in SST contrast also drives a decline in the reflectivity of the low clouds in the subsiding region and an increase in the reflectivity of the clouds in the rising region. An increase in climate sensitivity is driven mostly by the decreased efficiency of the emission from the subsiding region to cool the system.

An interesting aspect of these Tropic-World experiments for real-world global warming is the robust expectation that warm tropical regions will warm faster than cooler tropical regions. Warm tropical regions control the atmospheric climate of the tropics because in warm regions deep convection occurs that provides the convective heating for the atmosphere and constrains the atmospheric temperature. The warm SST regions of the tropics have also been shown to be the key regions for controlling the global response to tropical changes (Dong et al., 2019). Zhou et al. (2016) have shown that increased tropical SST contrast can slow down global warming, if it results in a net increase in the solar radiation reflected by low clouds. In these experiments we did not see that effect on the average climate because the effect of increasing inversion strength on low cloud albedos is offset by the thermodynamic effect of warming temperatures. How the changing clear-sky greenhouse effect interacts with cloud feedbacks in a warming climate is likely highly dependent on the cloud parameterizations in the model, and requires continuing study. Observational studies suggest that the thermodynamic effect on low clouds is very important (McCoy et al., 2017; Qu et al., 2015). Myers & Norris (2016) suggest on the basis of observations that the dynamic and thermodynamic effects on tropical low cloud fraction should approximately cancel, yet give a small net positive shortwave cloud feed-

back, approximately in agreement with the low cloud feedbacks in the present study of Tropic-World.

References

Albern, N., Voigt, A., Buehler, S. A., & Grutzun, V. (2018). Robust and nonrobust impacts of atmospheric cloud-radiative interactions on the tropical circulation and its response to surface warming [Journal Article]. *Geophys. Res. Lett.*, *45*(16), 8577-8585. Retrieved from `<GotoISI>://WOS:000445612500077` doi: 10.1029/2018gl079599

Anderson, J. L., Balaji, V., Broccoli, A. J., Cooke, W. F., Delworth, T. L., Dixon, K. W., ... Dev, G. G. A. M. (2004). The new gfdl global atmosphere and land model am2-lm2: Evaluation with prescribed sst simulations [Journal Article]. *J. Climate*, *17*(24), 4641-4673.

Becker, T., Stevens, B., & Hohenegger, C. (2017). Imprint of the convective parameterization and sea-surface temperature on large-scale convective self-aggregation [Journal Article]. *J. Adv. Model. Earth Sys.*, *9*(2), 1488-1505. Retrieved from `<GotoISI>://WOS:000406239300040` doi: 10.1002/2016ms000865

Birner, T. (2010). Residual circulation and tropopause structure [Journal Article]. *Journal of the Atmospheric Sciences*, *67*(8), 2582-2600. Retrieved from `https://journals.ametsoc.org/doi/abs/10.1175/2010JAS3287.1` doi: 10.1175/2010jas3287.1

Bony, S., Stevens, B., Coppin, D., Becker, T., Reed, K., Voigt, A., & Medeiros, B. (2016). Thermodynamic control of anvil-cloud amount [Journal Article]. *Proc. Nat. Acad. Sci. U. S. A.*, *113*(32), 8927-8932. doi: doi:10.1073/pnas.1601472113

Bretherton, C. S. (2015). Insights into low-latitude cloud feedbacks from high-resolution models [Journal Article]. *Phil. Trans. Roy. Soc. A*, *373*(2054). Retrieved from `<GotoISI>://WOS:000366270500002` doi: 10.1098/rsta.2014.0415

Bretherton, C. S., & Blossey, P. N. (2014). Low cloud reduction in a greenhouse-warmed climate: Results from lagrangian les of a subtropical marine cloudiness transition [Journal Article]. *Journal of Advances in Modeling Earth Systems*, *6*(1), 91-114. Retrieved from `<GotoISI>://WOS:000334866700007` doi: 10.1002/2013ms000250

Bretherton, C. S., Blossey, P. N., & Khairoutdinov, M. (2005). An energy-balance analysis of deep convective self-aggregation above uniform sst [Journal Article]. *J. Atmos. Sci.*, *62*(12), 4273-4292. Retrieved from `<GotoISI>://000234419800009`

Brient, F., & Bony, S. (2013). Interpretation of the positive low-cloud feedback predicted by a climate model under global warming [Journal Article]. *Climate Dynamics*, *40*(9-10), 2415-2431. Retrieved from `<GotoISI>://WOS:000318278700016` doi: 10.1007/s00382-011-1279-7

Chou, M. D., Ridgway, W. L., & Yan, M. M. H. (1993). One-parameter scaling and exponential-sum fitting for water vapor and co/sub 2/ infrared transmission functions [Journal Article]. *J. Atmos. Sci.*, *50*(14), 2294-2303.

Clough, S. A., Shephard, M. W., Mlawer, E., Delamere, J. S., Iacono, M., Cady-Pereira, K., ... Brown, P. D. (2005). Atmospheric radiative transfer modeling:

a summary of the aer codes [Journal Article]. *J. Quanti. Spectros. Rad. Trans.*, *91*(2), 233-244. Retrieved from `<GotoISI>://WOS:000224785800010` doi: 10.1016/j.jqsrt.2004.05.058

Coppin, D., & Bony, S. (2015). Physical mechanisms controlling the initiation of convective self-aggregation in a general circulation model [Journal Article]. *J. Adv. Model. Earth Systems*, *7*(4), 2060-2078. Retrieved from `<GotoISI>://WOS:000368739800030` doi: 10.1002/2015ms000571

Coppin, D., & Bony, S. (2017). Internal variability in a coupled general circulation model in radiative-convective equilibrium [Journal Article]. *Geophys. Res. Lett.*, *44*(10), 5142-5149. Retrieved from `<GotoISI>://WOS:000404131900090` doi: 10.1002/2017gl073658

Coppin, D., & Bony, S. (2018). On the interplay between convective aggregation, surface temperature gradients, and climate sensitivity [Journal Article]. *J. Adv. Model. Earth Sys.*, *10*(12), 3123-3138. Retrieved from `https://agupubs.onlinelibrary.wiley.com/doi/abs/10.1029/2018MS001406` doi: doi:10.1029/2018MS001406

Cronin, T. W., & Wing, A. A. (2017). Clouds, circulation, and climate sensitivity in a radiative-convective equilibrium channel model [Journal Article]. *J. Adv. Model. Earth Sys.*, *9*(8), 2883-2905. Retrieved from `<GotoISI>://WOS:000422718400005` doi: 10.1002/2017ms001111

Dee, D. P., Uppala, S. M., Simmons, A. J., Berrisford, P., Poli, P., Kobayashi, S., . . . Vitart, F. (2011). The era-interim reanalysis: configuration and performance of the data assimilation system [Journal Article]. *Quart. J. Royal Met. Soc.*, *137*(656), 553-597. Retrieved from `<GotoISI>://WOS:000290450900001` doi: 10.1002/qj.828

Delworth, T. L., Broccoli, A. J., Rosati, A., Stouffer, R. J., Balaji, V., Beesley, J. A., . . . Zhang, R. (2006). Gfdl's cm2 global coupled climate models. part i: Formulation and simulation characteristics [Journal Article]. *J. Climate*, *19*(5), 643-674. Retrieved from `<GotoISI>://WOS:000236668000002` doi: 10.1175/jcli3629.1

Dong, Y., Proistosescu, C., Armour, K. C., & Battisti, D. S. (2019). Attributing historical and future evolution of radiative feedbacks to regional warming patterns using a green's function approach: The preeminence of the western pacific [Journal Article]. *J. Climate*, *32*(17), 5471-5491. Retrieved from `<GotoISI>://WOS:000477890200001` doi: 10.1175/jcli-d-18-0843.1

Harrop, B. E., & Hartmann, D. L. (2012). Testing the role of radiation in determining tropical cloud-top temperature [Journal Article]. *J.Climate*, *25*(17), 5731-5747. Retrieved from `<GotoISI>://WOS:000308633500006` doi: 10.1175/jcli-d-11-00445.1

Harrop, B. E., & Hartmann, D. L. (2015). The relationship between atmospheric convective radiative effect and net energy transport in the tropical warm pool [Journal Article]. *Journal of Climate*, *28*(21), 8620-8633. Retrieved from `<GotoISI>://WOS:000363766200019` doi: 10.1175/jcli-d-15-0151.1

Harrop, B. E., & Hartmann, D. L. (2016). The role of cloud radiative heating in determining the location of the itcz in aquaplanet simulations [Journal Article]. *J. Climate*, *29*(8), 2741-2763. Retrieved from `<GotoISI>://WOS:000373359600001` doi: 10.1175/jcli-d-15-0521.1

Hartmann, D. (2016). *Global physical climatology* (2nd ed.) [Book]. Elsevier.

Hartmann, D., Blossey, P., & Dygert, B. (2019a). Convection and climate: What have we learned from simple models and simplified settings? [Journal Article]. *Curr. Clim. Change Rep.*, *5*(3), 196-206. Retrieved from `https://doi.org/10.1007/s40641-019-00136-9` doi: 10.1007/s40641-019-00136-9

Hartmann, D., Blossey, P., & Dygert, B. (2019b). Convection and climate: What have we learned from simple models and simplified settings? [Journal Article]. *Curr. Clim. Change Rep.*, *5*(3), 196-206. Retrieved from `https://doi.org/`

788   10.1007/s40641-019-00136-9 doi: 10.1007/s40641-019-00136-9

789 Hartmann, D. L., & Berry, S. E.   (2017).   The balanced radiative effect of tropical
790   anvil clouds [Journal Article].   *J.Geophys. Res.-Atmos.*, *122*(9), 5003-5020.   Re-
791   trieved from `<GotoISI>://WOS:000402039000014` doi: 10.1002/2017jd026460

792 Hartmann, D. L., & Larson, K. (2002).   An important constraint on tropical cloud-
793   climate feedback [Journal Article].   *Geophys. Res Lett.*, *29*(20), 1951-1954.   doi:
794   doi:10.1029/2002GL015835

795 Hartmann, D. L., Ockert-Bell, M. E., & Michelsen, M. L.   (1992).   The effect of
796   cloud type on earth's energy balance: global analysis [Journal Article].   *Journal of*
797   *Climate*, *5*(11), 1281-1304.   Retrieved from `<GotoISI>://WOS:A1992KX29200006`
798   doi: 10.1175/1520-0442(1992)005⟨1281:teocto⟩2.0.co;2

799 Hartmann, D. L., & Short, D. A.   (1980).   On the use of earth radiation budget
800   statistics for studies of clouds and climate [Journal Article].   *J. Atmos. Sci.*, *37*(6),
801   1233-50.

802 Held, I. M., Hemler, R. S., & Ramaswamy, V. (1993).   Radiative-convective equilib-
803   rium with explicit two-dimensional moist convection [Journal Article].   *J. Atmos.*
804   *Sci.*, *50*(23), 3909-3927.

805 Held, I. M., & Soden, B. J.   (2006).   Robust responses of the hydrological cycle to
806   global warming [Journal Article]. *J. Climate*, *19*(21), 5686-5699.

807 Held, I. M., Zhao, M., & Wyman, B. (2007). Dynamic radiative-convective equilibria
808   using gcm column physics [Journal Article]. *J. Atmos. Sci.*, *64*(1), 228-238.

809 Jeevanjee, N., & Fueglistaler, S.   (2020a).   On the cooling-to-space approximation
810   [Journal Article].   *J. Atmos. Sci.*, *77*(2), 465-478.   Retrieved from `<GotoISI>://`
811   `WOS:000508570000001` doi: 10.1175/jas-d-18-0352.1

812 Jeevanjee, N., & Fueglistaler, S. (2020b). Simple spectral models for atmospheric ra-
813   diative cooling [Journal Article].   *J. Atmos. Sci.*, *77*(2), 479-497.   Retrieved from
814   `<GotoISI>://WOS:000508570000002` doi: 10.1175/jas-d-18-0347.1

815 Klein, S., & Hartmann, D. (1993). The seasonal cycle of low stratiform clouds [Jour-
816   nal Article]. *J. Climate*, *6*(8), 1587-1606.

817 Kuang, Z. M., & Bretherton, C. S.   (2004).   Convective influence on the heat balance
818   of the tropical tropopause layer: A cloud-resolving model study [Journal Article].
819   *J. Atmos. Sci.*, *61*(23), 2919-2927.

820 Larson, K., & Hartmann, D. L.   (2003a).   Interactions among cloud, water vapor,
821   radiation, and large-scale circulation in the tropical climate. part ii: Sensitivity to
822   spatial gradients of sea surface temperature [Journal Article].   *J. Climate*, *16*(10),
823   1441-1455.

824 Larson, K., & Hartmann, D. L.   (2003b).   Interactions among cloud, water vapor,
825   radiation, and large-scale circulation in the tropical climate. part i: Sensitivity to
826   uniform sea surface temperature changes [Journal Article].   *J. Climate*, *16*(10),
827   1425-1440.

828 Loeb, N., Doelling, D. R., Wang, H., Su, W., Nguyen, C., Corbett, J., . . . Kato, S.
829   (2018). Clouds and the earth's radiant energy system (ceres) energy balanced and
830   filled (ebaf) top-of-atmosphere (toa) edition-4.0 data product [Journal Article].   *J.*
831   *Climate*, *31*(15 January 2018), 895-918. doi: doi.org/10.1175/JCLI-D-17-0208.1

832 Manabe, S., & Wetherald, R.   (1967).   Thermal equilibrium of the atmosphere with
833   a given distribution of relative humidity. [Journal Article]. *J. Atmos. Sci.*, *24*, 241-
834   259.

835 McCoy, D. T., Eastman, R., Hartmann, D. L., & Wood, R.   (2017).   The change
836   in low cloud cover in a warmed climate inferred from airs, modis, and era-
837   interim [Journal Article].   *J. Climate*, *30*(10), 3609-3620.   Retrieved from
838   `<GotoISI>://WOS:000401006100005` doi: 10.1175/jcli-d-15-0734.1

839 Mlawer, E. J., Taubman, S. J., Brown, P. D., Iacono, M. J., & Clough, S. A.
840   (1997).   Radiative transfer for inhomogeneous atmospheres: Rrtm, a validated
841   correlated-k model for the longwave [Journal Article].   *J Geophys. Res.-Atmos.*,

102(D14), 16663-16682.   Retrieved from `<GotoISI>://A1997XN38400019`   doi: 10.1029/97JD00237

Myers, T. A., & Norris, J. R.   (2016).   Reducing the uncertainty in subtropical cloud feedback [Journal Article].   *Geophys. Res. Lett.*, *43*(5), 2144-2148.   Retrieved from `<GotoISI>://WOS:000373109800044`   doi: 10.1002/2015gl067416

Petty, G.   (2006).   *A first course in atmospheric radiation* [Book].   Madison, Wisconsin: Sundog Publising.

Pierrehumbert, R.   (1995).   Thermostats, radiator fins and the local runaway greenhouse [Journal Article].   *J. Atmos. Sci.*, *52*, 1784-1806.

Popke, D., Stevens, B., & Voigt, A.   (2013).   Climate and climate change in a radiative-convective equilibrium version of echam6 [Journal Article].   *J. Adv. Model. Earth Sys.*, *5*(1), 1-14.   Retrieved from `<GotoISI>://WOS:000317833300001`   doi: 10.1029/2012ms000191

Qu, X., Hall, A., Klein, S. A., & DeAngelis, A. M.   (2015).   Positive tropical marine low-cloud cover feedback inferred from cloud-controlling factors [Journal Article].   *Geophysical Research Letters*, *42*(18), 7767-7775.   Retrieved from `http://dx.doi.org/10.1002/2015GL065627`   doi: 10.1002/2015GL065627

Ramanathan, V., Cess, R. D., Harrison, E. F., Minnis, P., Barkstrom, B. R., Ahmad, E., & Hartmann, D.   (1989).   Cloud-radiative forcing and climate: results from the earth radiation budget experiment [Journal Article].   *Science*, *243*(4887), 57-63.

Reed, K. A., Medeiros, B., Bacmeister, J. T., & Lauritzen, P. H.   (2015).   Global radiative-convective equilibrium in the community atmosphere model, version 5 [Journal Article].   *J. Atmos. Sci.*, *72*(5), 2183-2197.   Retrieved from `<GotoISI>://WOS:000353840100028`   doi: 10.1175/jas-d-14-0268.1

Renno, N. O., Emanuel, K. A., & Stone, P. H.   (1994).   Radiative-convective model with an explicit hydrologic cycle. 1. formulation and sensitivity to model parameters [Journal Article].   *Journal of Geophysical Research*, *99*(D7), 14429-41.

Renno, N. O., Stone, P. H., & Emanuel, K. A.   (1994).   Radiative-convective model with an explicit hydrologic cycle. 2. sensitivity to large changes in solar forcing [Journal Article].   *Journal of Geophysical Research*, *99*(D8), 17001-20.

Retsch, M. H., Mauritsen, T., & Hohenegger, C.   (2019).   Climate change feedbacks in aquaplanet experiments with explicit and parametrized convection for horizontal resolutions of 2,525 up to 5 km [Journal Article].   *J. Adv. Mod. Earth Sys.*, *11*(7), 2070-2088.   Retrieved from `https://agupubs.onlinelibrary.wiley.com/doi/abs/10.1029/2019MS001677`   doi: 10.1029/2019ms001677

Reynolds, R. W., Smith, T. M., Liu, C., Chelton, D. B., Casey, K. S., & Schlax, M. G.   (2007).   Daily high-resolution-blended analyses for sea surface temperature [Journal Article].   *J. Climate*, *20*(22), 5473-5496.   Retrieved from `<GotoISI>://WOS:000251236900001`   doi: 10.1175/2007jcli1824.1

Rodgers, C., & Walshaw, C.   (1966).   The computation of infrared cooling rate in planetary atmospheres [Journal Article].   *Quart. J. Roy. Meteor. Soc.*, *92*, 67-92.

Romps, D. M.   (2014).   An analytical model for tropical relative humidity [Journal Article].   *J. Climate*, *27*(19), 7432-7449.   Retrieved from `<GotoISI>://WOS:000342840400016`   doi: 10.1175/jcli-d-14-00255.1

Schneider, T., Kaul, C. M., & Pressel, K. G.   (2019).   Possible climate transitions from breakup of stratocumulus decks under greenhouse warming [Journal Article].   *Nature Geoscience*, *12*(3), 163-+.   Retrieved from `<GotoISI>://WOS:000460103000008`   doi: 10.1038/s41561-019-0310-1

Sherwood, S. C., Bony, S., & Dufresne, J. L.   (2014).   Spread in model climate sensitivity traced to atmospheric convective mixing [Journal Article].   *Nature*, *505*(7481), 37-+.   Retrieved from `<GotoISI>://WOS:000329163300019`   doi: 10.1038/nature12829

Tompkins, A. M.   (2001a).   On the relationship between tropical convection and sea

surface temperature [Journal Article]. *J. Climate*, *14*(5), 633-637. Retrieved from `<GotoISI>`://WOS:000167461300001 doi: 10.1175/1520-0442(2001)014⟨0633: otrbtc⟩2.0.co;2

Tompkins, A. M. (2001b). Organization of tropical convection in low vertical wind shears: The role of water vapor [Journal Article]. *J Atmos. Sci.*, *58*(6), 529-545. Retrieved from `<GotoISI>`://WOS:000167210400001 doi: 10.1175/1520-0469(2001)058⟨0529:ootcil⟩2.0.co;2

Wall, C. J., Hartmann, D. L., & Norris, J. R. (2019). Is the net cloud radiative effect constrained to be uniform over the tropical warm pools? [Journal Article]. *Geophys. Res. Lett.*, *46*(21), 12495-12503. Retrieved from `<GotoISI>`://WOS:000493702700001 doi: 10.1029/2019gl083642

Wing, A. A., & Emanuel, K. A. (2014). Physical mechanisms controlling self-aggregation of convection in idealized numerical modeling simulations [Journal Article]. *J. Adv. Model. Earth Sys.*, *6*(1), 59-74. Retrieved from `<GotoISI>`://WOS:000334866700005 doi: 10.1002/2013ms000269

Wing, A. A., Reed, K. A., Satoh, M., Stevens, B., Bony, S., & Ohno, T. (2018). Radiative-convective equilibrium model intercomparison project [Journal Article]. *Geosci. Model Dev.*, *11*(2), 793-813. Retrieved from `<GotoISI>`://WOS: 000426753800001 doi: 10.5194/gmd-11-793-2018

Wood, R., & Bretherton, C. S. (2006). On the relationship between stratiform low cloud cover and lower-tropospheric stability [Journal Article]. *J. Climate*, *19*(24), 6425-6432.

Zelinka, M. D., & Hartmann, D. L. (2010). Why is longwave cloud feedback positive? [Journal Article]. *J. Geophys. Res. Atmos.*, *115*. Retrieved from `<GotoISI>`://000281414400007 doi: D16117,10.1029/2010jd013817

Zhou, C., Zelinka, M. D., & Klein, S. A. (2016). Impact of decadal cloud variations on the earth's energy budget [Journal Article]. *Nature Geoscience*, *9*(12), 871-+. Retrieved from `<GotoISI>`://WOS:000390478700010 doi: 10.1038/ngeo2828